Evolution of the Frébouge polygenetic cone during the Holocene (Val Ferret, Mont Blanc Massif)

Catharina Dieleman[1], Philip Deline[2], Susan Ivy Ochs[3], Patricia Hug[4], Jordan Aaron[4], Marcus Christl[3], Naki Akçar[1]

5 [1]Institute of Geological Sciences, University of Bern, Switzerland
[2]EDYTEM Lab, University Savoie Mont Blanc, France
[3]Laboratory of Ion Beam Physics, ETH Zurich, Switzerland
[4]Geological Institute, ETH Zurich, Switzerland

10 *Correspondence to*: Catharina Dieleman (catharina.dieleman@unibe.ch)

Abstract. Proglacial settings in the Alps are typically polygenetic, often characterized by a complex and discontinuous interplay between glacial, fluvial, and gravitational processes. These processes yield high volume of sediments, which usually exceeds the transportation capacity. The excessive proglacial sediment load leads to accumulation on slopes, and thus, to subsequent failures such as debris flows. Such failures can occur unexpectedly and harm the villages and infrastructure in the vicinity of proglacial environments. The northern slopes of the Ferret and Veny valleys in the Mont Blanc Massif are home to several polygenetic cones and are a stunning field laboratory for the exploration of the interplay between the glacial, fluvial, and gravitational processes. This study investigates one of the active and well-preserved polygenetic cones in these valleys, namely the Frébouge cone, to disentangle the geomorphic processes that contributed to its formation, and to reconstruct its evolution. To achieve these goals, detailed field, and remote mapping, ^{10}Be surface exposure dating of different geomorphic features, and runout modelling with DAN3D® were applied. The geomorphological map revealed complex interactions of glacial, fluvial, debris flow, and rock and snow avalanche processes. The established chronology indicates two major fluxes of debris flows, the first one at ca. 2 ka, and the second at ca. 1 ka. In addition, a rock mass with a maximum volume of to 12 Mm^3 collapsed in the upper reaches of the cone at 1.3 ± 0.1 ka and overran the cone, travelling more than 100 m up onto the opposite valley slope. Afterwards, the Frébouge Glacier overrode the cone several times leaving moraines and till, reaching its maximum extent ca. 300 years ago. This study underscores the untwisting of the complex interaction of surface processes in the Alpine valleys, which are prone to hit the urban areas and infrastructure.

1 Introduction

Polygenetic landscapes are formed by the interplay of climate, tectonics, and surface processes that shape landscapes and threaten nearby populations and infrastructure (Bishop and Dobreva, 2017 and references therein). Such multi-process interaction is marvellously recorded in proglacial environments (Heckmann and Morche, 2019). Proglacial environments are often encountered in alpine landscapes (e.g., Penck and Brückner, 1909; Maizels, 1979; Costa et al., 2018; Carrivick et al.,

2019). They indicate a vicinity to a previous and active glacier margin because the retreat of alpine glaciers generally leads to the rise of new proglacial settings (Ballantyne, 2002; Slaymaker, 2011). Immediately after their nucleation, these environments are affected by the intermingling glaciofluvial, glaciolacustrine, and/or glaciomarine processes (e.g., Slaymaker, 2011). As

35   proglacial environments consist of unconsolidated sediments, which are often labile or unstable, they are associated with increased surficial activity characterized by a complex interaction of glacial, fluvial, and gravitational processes (Ballantyne, 2002).

In proglacial environments, the combination of different processes leads to high sediment production, which often exceeds the sediment discharge (e.g., Hallet et al., 1996). This misbalance between the sediment production and transport causes

40   accumulation, which is driven in part by sudden failures such as debris flows (Kamp and Owen, 2013; Carrivick et al., 2013), while rock, ice, and snow avalanches can get detached from the steep valley flanks (e.g., Akçar et al., 2012; Deline et al., 2015). As these mass movement processes can cause significant damage to the alpine villages and infrastructure located in the vicinity of proglacial environments, these processes are of great societal interest. Consequently, the investigation of the mechanisms governing the occurrence and behaviour of past failures, as well as their magnitudes and frequencies is critical

45   for improving hazard and risk assessments of alpine settlements and infrastructure, and in hazard mitigation (Prager et al., 2008; Ivy-Ochs and Schaller, 2009 among others).

The Italian Ferret Valley in the Mont Blanc Massif is a U-shaped glacial valley with steep valley flanks, where active morphodynamics and the combined influence of glacial, fluvial, and gravitational processes currently prevail (Figure 1). The Ferret Valley is characterized by many rock fall and rock avalanche deposits located beyond glacier tongues (Deline et al.,

50   2012, 2021). Therefore, it is a good example of a polygenetic landscape where the inhabitants and tourists visiting these valleys all around the year are under steady threat of natural hazards (Porter and Orombelli, 1981; Deline et al., 2004, 2012).

Previous work has only investigated single processes in the Ferret Valley (e.g. Porter and Orombelli, 1981; Deline et al., 2004). These have included analyses of the glacial history of the region, as well as investigations into previous mass movements at the site. During the Last Glacial Maximum, the Alps were covered by large ice streams (Bini et al., 2009). The subsequent

55   glacier retreat in the Ferret Valley was dated to 18.5 ± 1.1 ka based on cosmogenic ^{10}Be (Wirsig et al., 2016). Post-LGM glacier reconstructions show that glaciers were advancing to Courmayeur (Courmayeur advance suggested by Porter and Orombelli, 1982) at ca. 14 ka during the Daun Stadial (Serra et al., 2022 and references therein). A further glacier advance was attributed to either Egesen Stadial (13.5 – 12 ka; Ivy-Ochs, 2015) or an early Holocene re-advance at ca. 11 ka or 8.5 ka (Serra et al., 2022). The climate was cooling from 3 ka onwards resulting in new glacier advances culminating in the Little Ice

60   Age (LIA, 1250 – 1850 AD; Ivy-Ochs et al., 2009). Photographs and drawings document the extent of glaciers back to the early 20th century (Sacco, 1918; Gabinio, 1923).

The Ferret Valley is not only influenced by glaciations but also by mass movement processes. Rock avalanches and large rock falls with volumes from 10'000 m^3 to 10 Mm^3 were identified as occurring between 2.5 ka and 2007 (Deline, 2009; Deline and Kirkbride, 2009; Deline et al., 2012). In the upper part of the Ferret valley, the 1717 AD Triolet rock avalanche was studied

65   in detail (Figure 1). Deposits of this landslide were dated to 1742 AD by applying dendrochronology (Porter and Orombelli,

1980) and between 1717 AD and 1727 AD by lichenometry (Porter and Orombelli, 1980), which was later confirmed by surface exposure dating with cosmogenic [10]Be (Akçar et al., 2012, 2014). Another rock avalanche event in the Ferret Valley was observed at the toe of the Frébouge Glacier, which has taken place around 350 years ago (Porter and Orombelli, 1981), representing a part of the Frébouge polygenetic cone (Deline 2009). Finally, the Frébouge polygenetic cone was partially

70 covered by the Frébouge Glacier during the LIA (Deline, 2009). Frequent snow avalanches and debris flows fed by glacial runoff have been recorded over the past decades (Deline et al., 2004).

The Frébouge polygenetic cone thus provides a unique record of complex natural hazards such as rock avalanches, debris flows, snow, and ice avalanches, the future occurrence of which can constitute a danger for the inhabitants of this area. Hitherto, the processes on the Frébouge polygenetic cone have been considered independently, and their interactions have not been

75 studied in detail. In this paper, we present a holistic view of the polygenetic cone and explore all processes at once. This allows us to decipher the geomorphic processes and their interactions, and to understand the evolution of the Frébouge polygenetic cone. To achieve this, field mapping and remote sensing tools were applied. The chronology of this polygenetic cone was established by applying cosmogenic [10]Be surface exposure dating on moraines, debris flow deposits, and rock avalanche deposits. The dynamics of the Frébouge rock avalanche were investigated using the semi-empirical numerical model DAN3D.

80 **2 Study site**

The Frébouge polygenetic cone is located on the southern flank of the Mont Blanc Massif in the Ferret Valley in Italy. This valley is close to the Swiss border and is a tributary valley of the Aosta Valley (Figure 1). The northern valley flank is about 2000 m above today's valley floor and consists of porphyric Mont Blanc Granite (Marro, 1986; Porter and Orombelli, 1980; swisstopo, 2015). On the southern flank limestones, schists, and flysch from the Jurassic, Helvetic, and Cretaceous units are

85 outcropping (Porter and Orombelli, 1980; swisstopo, 2015). The Frébouge cone is about 1.2 km long, between 1650 and 2150 m a.s.l., with a mean slope angle of 17° and a surface area of ~1 km^2 (Figures 1 and 2).
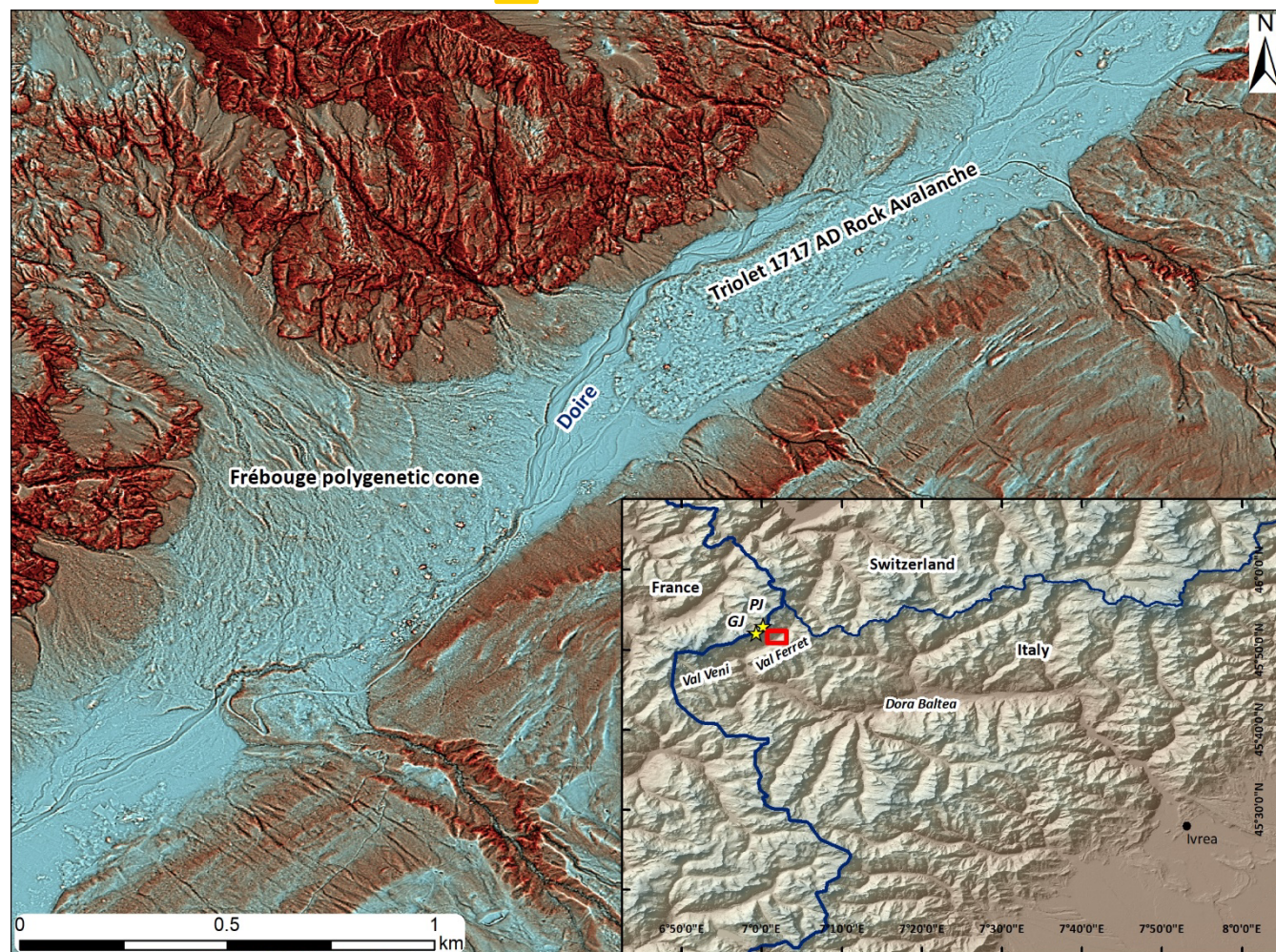
Figure 1: The Red Relief Image Map (RRIM) of the Frébouge polygenetic cone and the 1717AD Triolet rock avalanche. The inset shows the location of the study within the Alpine realm © European Union, Copernicus Land Monitoring Service 2023, European Environment Agency (EEA). PJ = Petites Jorasses and GJ = Grandes Jorasses.

Two main rock avalanche deposits are located on the south and east sides of the cone. A first rock avalanche would have occurred between AD 991 and AD 1154 based on radiocarbon dating of wood recovered by an open-framework structure sheet of granite boulders with a thickness between 1 m and 5 m; this rock avalanche that detached from the Frébouge Glacier cirque and ran up 100 – 140 m up on the other valley flank (Deline, 2009). The second rock avalanche deposit is 1 – 2 m in thickness except for the eastern part where it reaches a thickness larger than 4 m (Deline, 2009). The time of deposition was estimated to be AD 1530 based on lichenometry (Giambastiani, 1983). The large granite boulders deposited on the southern valley flank were previously interpreted to be of glacial origin (e.g., Sacco, 1918). The front of the Frébouge Glacier is now located high above the cone, at 2700 m a.s.l., but reached the tip of the cone at the beginning of the 20th century (Sacco 1918; Gabinio, 1923). Moraines on top of the fan deposits indicate the extent during the LIA (Deline, 2009). In the past decades, the fan was

4

100   mainly influenced by debris flows (Deline et al., 2004) and snow avalanches; ice avalanches detached from the glacier front
       in 2002 and possibly in 1968 (Deline et al., 2002). Upstream of the Frébouge cone, the deposit of the 1717 AD Triolet rock
       avalanche and the recent morainic complexes of the Triolet and Pré de Bar Glaciers can be found (Deline and Kirkbride, 2009).

Figure 2: Photograph of the Frébouge polygenetic cone, on which the moraines A, B, and C are located (indicated by the black lines).
View towards the north.

5

3 ~~Methodology~~

3.1 Geomorphological mapping

Geomorphological mapping provides a detailed understanding of landscape shaping processes (Griffith et al., 2011;

110 Seijmonsbergen, 2013). In this study, the mapping campaign was conducted in August 2020 and the software Fieldmove®
was used. The digital terrain model (DTM) of the Aosta Valley with a 2m resolution was downloaded from the Servizi
Cartografici SCT (mappe.partout.it/pub/geonavitg/geodownload.asp). Out of the DTM a shaded relief, a slope, and an aspect
map were created using the software ArcGISPro®. Landforms were mapped in detail in the field and their extensions were
tracked with a GPS. For remote digital mapping, high-resolution aerial photographs, which were taken with an unmanned

115 aerial vehicle, were then used to create a high-resolution digital elevation model (DEM) and orthophotograph of the study
area. The corresponding flight missions were planned in Litchi Mission Hub® (flylitchi.com/hub). The flight altitude was set
to 200 m above ground. In order to achieve ca. 80 % side overlap the spacing between the flight lines was 100 m. The camera
was in an orthogonal position and captured nadir images every 2.5 s. Three flight missions were conducted in total, two
covering the lower part of the cone and one the upper part. The photographs were processed in the photogrammetry software

120 Agisoft Metashape®.

3.2 Surface exposure dating

In this study, 16 samples from the surface of granitic boulders on the Frébouge cone were collected with a hammer and chisel
following the protocol described in previous studies (e.g., Akçar et al., 2011). Information on the geomorphological landform,
lithology, geographical position, dimensions, sample thickness, and shielding factors are provided in Table 1. Nine samples

125 were taken from different parts of the rock avalanche (RA) (Figure 3). Three samples were collected from boulders on the
outermost Moraine-A (Figures 2 and 3). Four samples were taken from the debris flow deposits in the north-eastern and in the
south-western areas of the Frébouge cone. The thickness of the collected samples varies between 3 and 5 cm (Table 1).

Table 1: Sample information of the investigated geomorphologic features from the Frébouge polygenetic cone.

Sample Name	Geomorphological landform	Sampling year	Latitude °N	Longitude °E	Altitude (m a.s.l.)	Dimensions LxWxH (m)	Sample thickness (cm)	Shielding Factor*
FREB-1	RA	2012	45.85799	7.03401	1732	1.7 x 1.5 X 1.2	3	0.9432
FREB-2	RA	2012	45.85799	7.03409	1732	2.8 x 1.8 x 1.6	3	0.9432
FREB-3	RA	2012	45.85792	7.03413	1733	4.0 x 1.6 x 1.9	5	0.9432
FREB-4	RA	2012	45.85795	7.03416	1733	3.6 x 1.5 x 1.6	4	0.9432
FREB-5	RA	2012	45.85196	7.02843	1720	2.6 x 2.2 x 2.1	4	0.9582
FREB-6	RA	2012	45.85320	7.02743	1697	9.7 x 6.0 x 4.6	4	0.9588
FREB-7	RA	2012	45.85263	7.02729	1697	5.8 x 3.6 x 2.1	5	0.9588
FREB13	RA	2020	45.85732	7.03097	1721	4.2 x 3.0 x 2.8	5	0.9572
FREB14	RA	2020	45.85817	7.03119	1736	14.0 x 6.5 x 3.0	4	0.9559
FREB8	Moraine	2020	45.86130	7.03052	1797	5.0 x 4.0 x 3.0	4	0.9270
FREB9	Moraine	2020	45.86115	7.03054	1794	3.5 x 2.5 x 1.4	3	0.9270
FREB10	Moraine	2020	45.86025	7.03057	1783	5.3 x 3.1 x 3.0	4	0.9448
FREB11	DF north	2020	45.86224	7.03242	1765	1.2 x 1.2 x 1.1	3.5	0.9287
FREB12	DF north	2020	45.86234	7.03242	1764	1.2 x 0.9 x 0.9	5	0.9287
FREB15	DF south	2020	45.85583	7.02423	1705	1.6 x 1.2 x 0.7	5	0.9472
FREB16	DF south	2020	45.85604	7.02525	1711	1.0 x 0.7 x 0.6	4	0.9523

topographic shielding based on Dunne et al. (1999).

130 The sample preparation for cosmogenic [10]Be took place at the Surface Exposure Dating Laboratory of the University of Bern. To separate and purify the collected samples a modified version of the technique introduced by Kohl and Nishiizumi (1992) was applied (Akçar et al., 2017). The [10]Be of the purified quartz was extracted according to the protocol of Akçar et al. (2012) for the AMS (Accelerator Mass Spectrometry) measurements at ETH Zurich. The samples were processed in batches of nine samples and one full process blank. The [10]Be/[9]Be ratios of FREB-1 to FREB-7 were measured on the 0.5 MV TANDY and

135 the samples FREB-8 to FREB-16 on the MILEA AMS facilities at ETH Zurich (Kubik and Christl, 2010; Christl et al., 2013; Maxeiner et al., 2019). The measured [10]Be/[9]Be ratios were corrected with a long-term weighted average full process blank of $(2.82 \pm 0.29) \times 10^{-15}$ for FREB-1 to FREB-7 and of $(3.05 \pm 0.34) \times 10^{-15}$ for FREB-8 to FREB-16, respectively. The exposure ages were then calculated with the online exposure age calculator, formerly known as CRONUS-Earth online calculator, referenced to 07KNSTD (hess.ess.washington.edu/math/v3/v3_age_in.html; version 3; Balco et al., 2008). The production

140 rates of the cosmogenic nuclides were locally scaled by applying the time-dependent Lal (1991) / Stone (2000) scheme. For the exposure age calculations, a half-live of 1.39 Ma was applied (Chmeleff et al., 2010; Korschinek et al., 2010). Furthermore, the topographic shielding based on Dunne et al. (1999), the sample thickness using an attenuation length of 160 g/cm^2, and the rock density of 2.65 g/cm^3 were considered for the calculations. The erosion rate of 1 mm/ka was estimated based on André

145   (2002). We did not correct the exposure ages for the snow coverage. In addition, all the landform ages provided in the following text were calculated by the probabilistic cosmogenic age analysis tool published by Dortch et al. (2022).

3.3 Volume estimation and runout modelling with DAN3D

The Frébouge rock avalanche was simulated using the semi-empirical DAN3D (dynamic analysis 3D) model proposed by McDougall and Hunger (2004). This model is a path-averaged Lagrangian implementation of the equations of motion which can simulate non-hydrostatic internal pressure distributions. It has been used by previous researchers to analyze a large number

150   of rock avalanches (e.g. Aaron & McDougall 2019). Dan3D requires the following input parameters: The topography of the surface overrun by the rock avalanche (here termed the path topography), the thickness and distribution of the source volume, as well as the rheology type and rheological parameters. The rheological parameters are typically calibrated with back-analysis (Aaron and Hungr, 2016; Aaron et al., 2019).

A modified present-day DEM (described below) was used for the path topography, however the source area of the Frébouge

155   rock avalanche is unclear. We therefore tested two different release areas located at the Grandes Jorasses (GJ) and Petites Jorasses (PJ) (Figure 1), as both appear to be plausible source zones. To estimate the source volume, we first estimated the deposit volume and then reduced it by 25% to account for bulking (Hungr and Evans, 2004). We estimated the deposit volume by manually modifying a recent DEM based on the thickness of the deposits estimated while mapping as well as a geomorphic analysis of the deposit (Grämiger et al., 2016). A small hill in the southwestern part of the Frébouge cone was due to its small

160   volume included in the volume estimate (Figure 3). Subtracting the present-day DEM from the reconstructed pre-failure topography yielded the landslide deposit volume.

We applied a multi-step calibration process to select the best rheology and parameter values for the numerical simulations. In the first step, a single material and the Voellmy rheology was used to simulate the runout of the basal resistance experienced by the Frébouge rock avalanche. This rheology is well-suited for extremely rapid, flow-like mass movements (Aaron &

165   McDougall 2019; Aaron et al., 2019). Multiple combinations of friction and turbulence coefficients can result in the same runout extent (Aaron et al., 2019), however in the present work one valid parameter set was sufficient as the goal was to verify the volume estimates and compare different release areas. Therefore, the turbulence coefficient was kept constant at 500 m/s^2 and the friction coefficient was varied between 0.1 and 0.25 (simulations V1 to V4, Table 2) to reproduce the observations made in the field. Four different quantities were suggested to compare DAN3D simulations with field observations (Aaron et

170   al., 2019). These are the impact area, the estimated volume in a certain area, the depth of the deposit at a certain point, or the flow velocity at a certain point. For the Frébouge rock avalanche the calibration with the landslide impact area was applied because it can be assessed by the geomorphological mapping. The internal friction angle was kept constant at 35° and a bulked unit weight of 20 kN/m^3 was used.

Table 2: Input parameters for the rock avalanche modelling using DAN3D.

Simulation	Material Type	Behaviour	Friction Angle (°)	Friction Coefficient	Tubulence Coefficient (m/s²)	Source
V1	Uniform	Voellmy	-	0.1	500	Aaron and McDougall (2019)
V2	Uniform	Voellmy	-	0.15	500	Aaron and McDougall (2019)
V3	Uniform	Voellmy	-	0.2	500	Aaron and McDougall (2019)
V4	Uniform	Voellmy	-	0.25	500	Aaron and McDougall (2019)
Multimat	Glacier	Frictional	8	-	-	Sosio et al. (2012)
	Bedrock	Frictional	20	-	-	Aaron (2017)
	Sediment	Voellmy	-	500	500	V3, Aaron and McDougall (2019)

175

In the second step of the model calibration, we used the results from the first step to perform a simulation with multiple materials (termed the 'Multimat simulation' herein). The use of multiple materials is recommended by Aaron et al. (2022) for cases that interact with a variety of path materials during their motion, as this captures the emplacement process more realistically. The path materials for the Frébouge cone were the glacier, bedrock, and saturated sediments. For the bedrock and
180 the glacier, frictional rheology with values from previous studies was utilized (Sosio et al. 2012; Aaron et al. 2022), whereas for the saturated sediment the calibrated Voellmy parameters from step 1 were applied. The input parameters for the runout modeling are summarized in Table 2.

4. Results

4.1 Geomorphology of the Frébouge cone

185 On the Frébouge cone, different types of landforms and deposits were identified (Figure 3). These include moraines, levees, and debris flow channels. Glacial deposits such as till and erratic boulders, debris flow sediments, hummocky deposits, deposits of a rock avalanche, sediments from an alluvial plain, and deposits from snow avalanches were also mapped in the field. Along the cone, glacial meltwater and debris flow events incised about 50 m wide channels. In the southernmost part, the debris flow in 2003 deposited levees on both sides of the channel, which are up to 2 m in height and about 300 m in length (Figure 3). The
190 debris flow deposit is moderately sorted. The grain sizes range from sand to blocks. Most of the clasts are subangular to subrounded and are on average 15 cm in diameter. Furthermore, in the channels white coloured and fresh to slightly weathered debris is deposited. This sediment originates from the daily load of the creeks. The extent of the debris flow event can be reconstructed based on the colour difference to the surrounding.

9
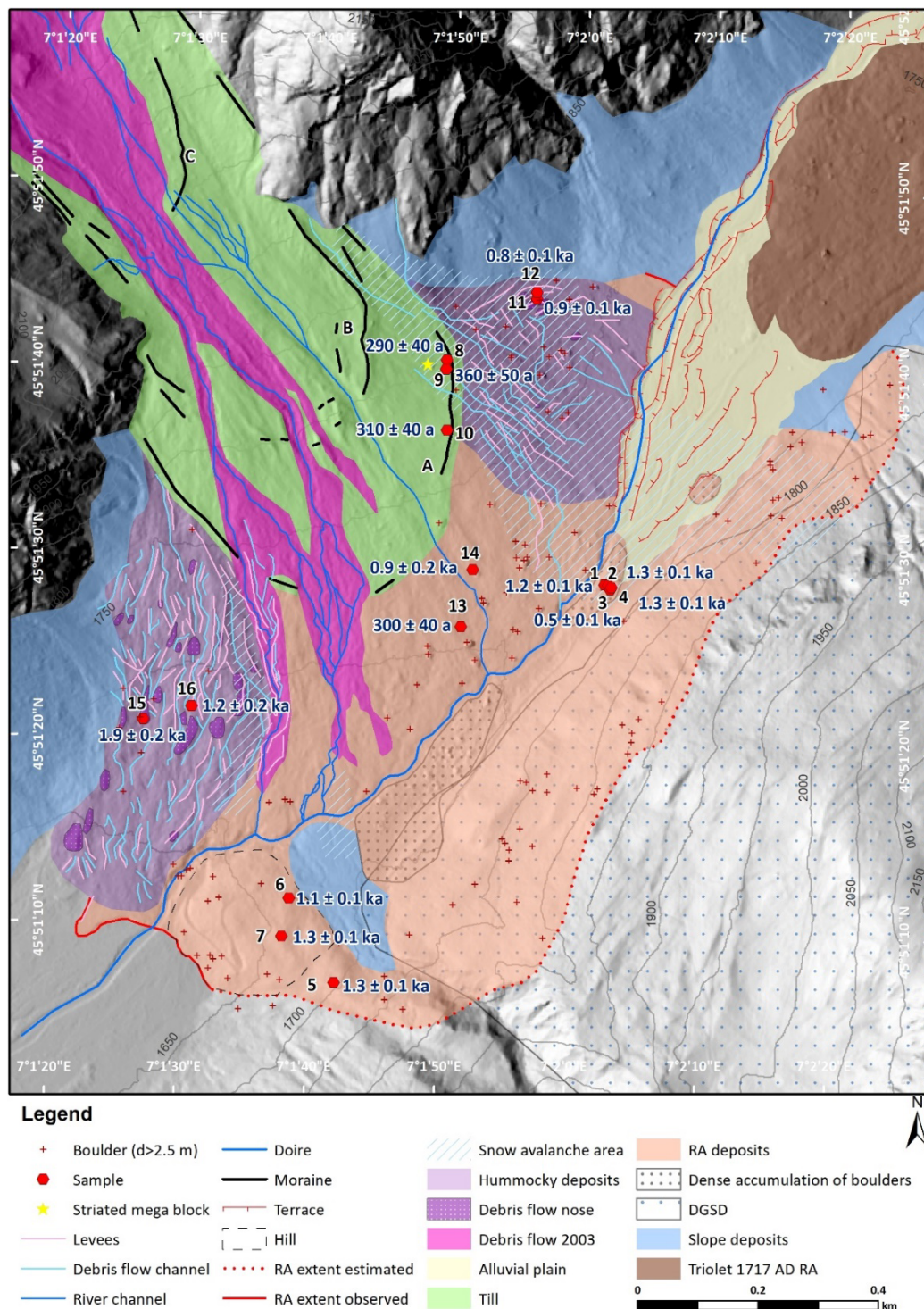
Figure 3: Surficial geology map of the study area (RA: Rock Avalanche, DGSD: Deep-seated gravitational slope deformation). The red hexagons indicate the locations of the sampled boulders, the black numbers the number of the sample, and the blue numbers the exposure age of the sampled boulder ©Servizi Cartografici SCT.

The southwestern and northeastern part of the Frébouge cone is characterized by hummocky deposits consisting of a complex network of channels, levees, and debris flow noses (Figure 3). The longest channel is about 500 m in length and 15 m in width.

200 These channels were formed by incision of the debris flow into the surface. Levees are elongated landforms lying on the side of the channels. The debris flow noses can be up to 60 m long, 25 m wide, and 10 m high (Figure 4). These noses are structures with a blocky terminus. On the Frébouge cone, the levees and the debris flow noses are difficult to distinguish. Therefore, all landforms with a clear blocky end were classified as debris flow noses regardless of their length. Elongated geomorphic features on the other hand were classified as levees. The sediment of the levees and the debris flow noses are mostly well-

205 sorted, and their grain size is between cobbles and blocks. The clasts are subrounded. Within unweathered deposits, sand and finer-grained sediments were observed.

Figure 4: Photographs of the debris flow deposits. A) A debris flow nose in the southwestern part of the cone. B) Sampled boulder FREB-15. C) Sampled boulder FREB-11.

In addition, the area with the hummocky deposits is strongly vegetated and forested. In the northeastern part, many levees and debris flow noses are up to 2 m high, whereas they are less than 1 m in the southwestern part. In the area of the debris flow noses the forest is less dense. The channels and levees show a complex interaction. Older levees and channels are cut by

11

215 younger ones and towards the center of the cone they tend to be longer than at the sides, where they are stronger segmented. The main orientation of the channels and levees in the southwestern part is NE-SW and NNW-SSE in the north-eastern part.

Rock avalanche deposits dominate the lower part of the cone, where debris forms a chaotic deposit (Figure 3). The rock avalanche deposit consists of weathered, unsorted, and angular to subangular clasts with a grain size between sand and blocks. Two dense accumulations of granite boulders and an accumulation of boulders larger than 2.5 m in diameter are located at the distal zone of the cone. The largest boulder reaches a height of 10 m (Figure 5). In the dense accumulation of granite boulders,

220 smaller blocks are also observed. A 2 m high rim marks the extent of the rock avalanche deposit on the sides of the cone, whereas the southeastern limit of the rock avalanche deposit is not determined by a clear rim. Therefore, this limit was reconstructed based on the frequency of granitic boulders along the slope. In this part, the deposit has a thickness of 0.5 m.

225 **Figure 5: Photographs of the boulders deposited by the rock avalanche. A) A large and ca. 5 m high boulder. B) Sampled boulder FREB-14. C) Sampled boulder FREB-13.**

On the northern edge of the cone and south of the river, an alluvial plain with a length of more than 400 m and a width of 250 m is observed (Figure 3). Only a few blocks are exposed there. The plain is veined by small, inactive channels and terraces. An accumulation of blocks delineates the plain in the south and the deposit of the 1717 AD Triolet rock avalanche in the north.

230 Till dominates the topmost part of the cone. Three broad-crested lateral and terminal moraines are present, which are disrupted

by river channels in the central part (Figures 2 and 3). Outermost Moraine-A at an elevation between 1900 and 1750 m a.s.l. has a length of ca. 300 m and a height of 2-3 m. Moraine-B represents a latero-terminal moraine starting at an elevation of 1950 m a.s.l. descending to 1815 m a.s.l. The north-eastern ridge is 500 m long and 2 m in height. On the southwestern side the ridge is only preserved discontinuously. Moraine-C is found at an elevation between 2125 and 1965 m a.s.l. This latero-
235 terminal moraine is 380 m long and 1.5 m high. These three moraines are composed of weathered and poorly sorted till. The grain sizes vary from clay to large blocks, which are of granitic composition. The clasts are subangular to subrounded in shape and mainly striated. Furthermore, in the upper part of the cone, large and fractured blocks with evidence of glacial erosion are present. They are up to 4 m high, polished, rounded, and striated on the upslope side and angular in shape on the downslope side.

240 The Frébouge cone has been frequently affected by snow avalanches (Figure 3). Indicators such as freshly broken boulders are observed. Furthermore, many boulders were displaced for a few meters and thereby left behind a track, which preserved their original depositional position in the field. In addition, fallen trees and forest aisles were found in this area.

The secondary slope movements such as small-scaled failures, debris cones, and talus slopes interact with the Frébouge cone. The south-eastern side of the valley could be affected by a deep-seated gravitational slope deformation (DGSD) and snow
245 creep, which could be indicated in the field by bent trees.

4.2 Chronology of the Frébouge cone

At the Frébouge cone, 16 rock surface samples in total were collected from granitic boulders and processed for the analysis of cosmogenic [10]Be (Figure 5; Tables 1 and 3). Four samples were taken from the northeastern rock avalanche deposits (FREB-1 to FREB-4), three from the southwestern part (FREB-5 to FREB-7), and two from the center of the rock avalanche deposits
250 (FREB-13 and FREB-14) (Figure 5). Three samples were taken from moraine-A (FREB-8 to 10). From stabilized debris flow noses, two samples were taken in the northeastern part (FREB-11 and FREB-12), and two from the southwestern part (FREB-15 and FREB-16) (Figure 4). The results of the [10]Be measurements and the calculated exposure ages are shown in table 3.

Table 3: Cosmogenic [10]Be data of the samples and calculated exposure ages

Sample Name	Quartz dissolved (g)	[9]Be spike (mg)	[10]Be/[9]Be Ratio (x10^{-14})	Uncertainty (%)	Nb of [10]Be (x10^3 atoms per g)	[10]Be Exposure Age (years)
FREB-1	48.8903	0.1481	9.96	10.1	19.59 ± 2.04	1200 ± 100
FREB-2	50.3040	0.1480	4.53	9.9	8.35 ± 0.88	500 ± 70
FREB-3	50.1357	0.1484	10.62	6.3	20.45 ± 1.32	1300 ± 100
FREB-4	54.2222	0.1483	11.35	8.2	20.23 ± 1.70	1300 ± 100
FREB-5	49.9940	0.1489	10.34	5.8	20.02 ± 1.19	1300 ± 100
FREB-6	50.7657	0.1475	8.55	9.7	16.05 ± 1.61	1100 ± 100
FREB-7	50.6426	0.1483	10.21	7.7	19.45 ± 1.54	1300 ± 100
FREB13	50.1818	0.1985	2.09	9.5	4.72 ± 0.53	300 ± 40
*FREB14	50.1102	0.1999	4.93	8.2	14.36 ± 3.22	900 ± 200
*FREB14_2			6.64	9.7		
FREB8	49.9992	0.2034	2.09	10.8	4.85 ± 0.62	290 ± 40
FREB9	49.9712	0.2041	2.54	8.5	6.10 ± 0.59	360 ± 50
FREB10	50.1080	0.1957	2.29	9.2	5.18 ± 0.55	310 ± 40
FREB11	49.9800	0.1966	5.68	6.3	14.13 ± 0.94	900 ± 90
FREB12	49.9792	0.1978	5.02	5.6	12.47 ± 0.75	800 ± 80
FREB15	50.0302	0.1984	11.48	3.6	29.61 ± 1.10	1900 ± 200
*FREB16			9.15	9.6		
*FREB16_2	49.9732	0.1986	5.28	10.8	18.76 ± 2.77	1200 ± 200
*FREB16_3			7.18	8.6		

* >1 targets from the same sample were measured
Note: The reported blank ratio and the concentration are referenced to S2007N (Kubik and Christl, 2010; Christl et al., 2013; Maxeiner et al., 2019). AMS measurement errors are at 1σ level, including the statistical (counting) error and the error due to normalization of the standards and blanks. he error weighted average [10]Be/[9]Be full process blank ratio for the samples FREB-1 to 7 is (2.76 ± 0.18) x 1e-15 and (3.05 +- 0.34) x 1e-15 for the samples FREB-8 to 16. FREB-1 to 7 were measured in 2013 in Tandy, and the others in 2020 in Milea.

255 The [10]Be/[9]Be ratios are between 2.09×10^{-14} and 11.48×10^{-14}. The relative measurement uncertainty of the [10]Be/[9]Be ratios ranges from 3 % to 11 %. The full process blank accounts for 2.48 % to 14.59 % of the measured [10]Be/[9]Be ratios. The calculated, blank corrected [10]Be concentrations vary between $(4.72 \pm 0.53) \times 10^3$ atoms/g and $(29.60 \pm 1.10) \times 10^3$ atoms/g. For the samples of the northeastern rock avalanche deposits surface exposure ages of 1200 ± 100, 500 ± 70, 1300 ± 100, and 1300 ± 100 years were calculated. The ages from the southwestern rock avalanche deposits are between 1100 ± 100 and 1300

260 ± 100 years and the ones from the center of the deposit have an age of 300 ± 40 and 900 ± 200 years. The probability density function plot of the exposure ages of the rock avalanche deposit indicates a mean age of 1300 ± 100 years; FREB-2 (500 ± 70

a) and FREB-13 (300 ± 40 a) were identified as outliers and excluded from the average age calculation (Figure 6). The surface exposure ages of the moraine samples are 290 ± 40, 360 ± 50, and 310 ± 40 years, with an average exposure age of 300 ± 40 years for the Moraine-A (Figure 6). The stabilized debris flow noses northeastern part were dated to 900 ± 90 and 800 ± 80

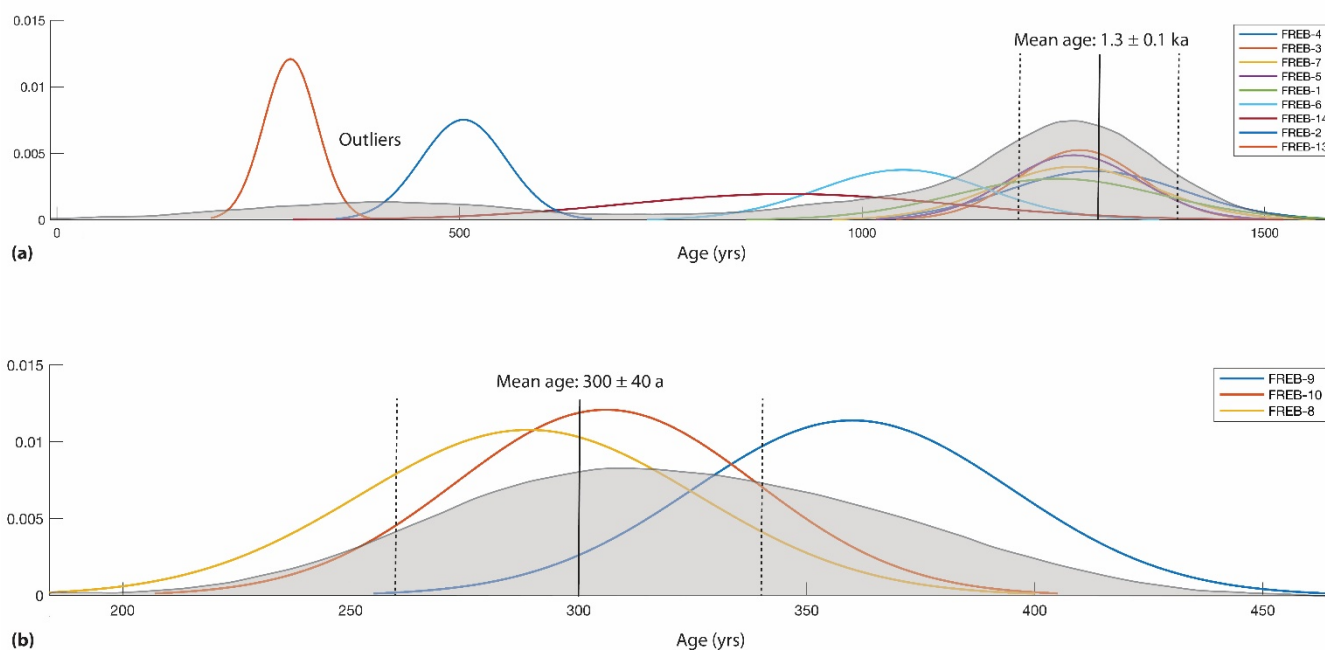265 years, whereas the ones in the southwestern part show ages of 1900 ± 200 and 1200 ± 200 years.

Figure 6: Probability density functions of the exposure ages from the rock avalanche (A) and the Moraine B and associated landform ages. Landform ages provided are calculated by the probabilistic cosmogenic age analysis tool published by Dortch et al. (2022).

270 **4.3 Volume Reconstruction and Runout Modelling**

The runout analysis allowed us to verify our geomorphic interpretation and place the mobility of the Frébouge rock avalanche into a broader context. The runout analysis is based on a volume reconstruction (Figure 7), which resulted in a deposit volume of 12 Mm^3, and a source volume of 9.5 Mm^3 (assuming 25% bulking). This volume was then used in the runout analysis, and the most relevant output parameters of the runout modeling are shown in Table 4, and final simulation results are given in

275 Figure 7. We find that V3 (Table 4) provides the best-fit simulation results for both modeled release areas (Grandes Jorasses (GJ) and the Petites Jorasses (PJ)). Further, the modeling revealed that the thickness and the extent of the deposit at the end of the simulation are similar regardless of which of the two release areas (GJ or PJ) are used.
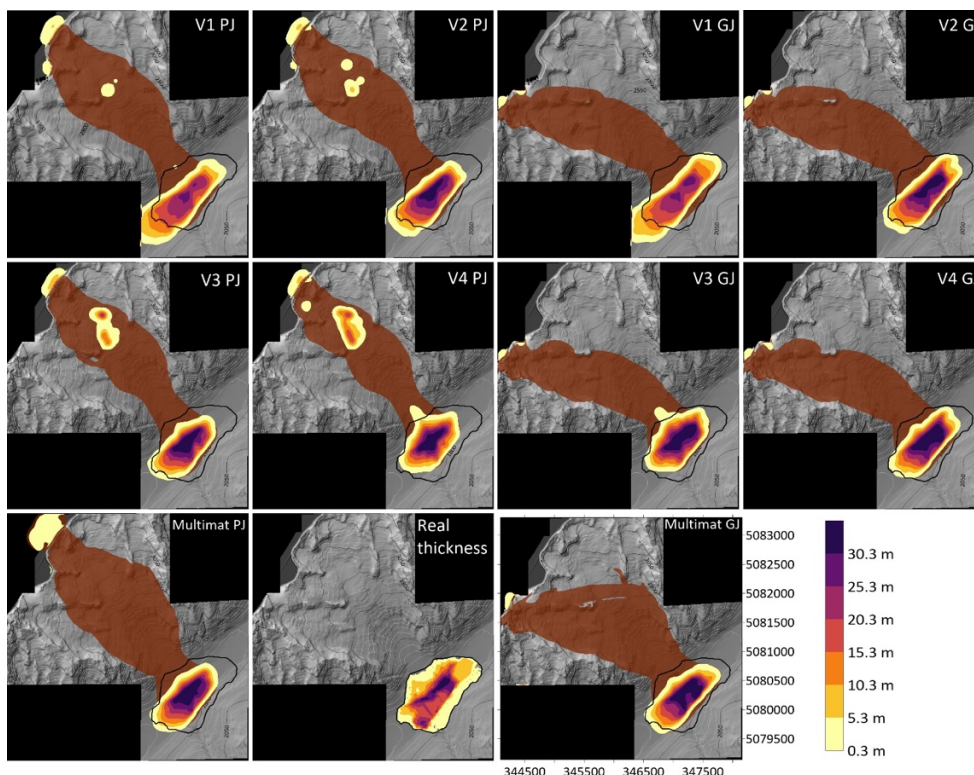
Figure 7: Comparison of the different simulations at their end. The comparison uses the extent and thickness of the rock avalanche deposit with Grandes Jorasses (GJ, left) and Petites Jorasses (PJ, right) as release areas. Displayed in brown is the impact area of the rock avalanche. The black line indicates the extent of the rock avalanche deposit mapped in the field the real thickness plot shows the thickness obtained during the topographic reconstruction.

The "Multimat" simulations, which separate out the effects of the various path materials encountered by the rock avalanche (glacial ice and saturated sediment), are based on the calibrated V3 parameters and literature values. As shown in Figure 7 and Table 4, the impact area is similar when compared to the one material simulation. Further, the "Multimat" simulations result in higher peak velocities and no material deposited in the upper catchment. Considering all these results, the most realistic simulation is the one using the "Multimat" parameters released from the GJ as this runout simulation of the rock avalanche is best-fitting with the field observations. Therefore, we build our discussion on these results.

Table 4: Output parameters of the rock avalanche modelling using DAN3D

Release Area	Simulation	Max. Deposit Thickness (m)	Max. Velocity (m/s)	Travel distance (vert./horiz., m)	Max. Run-up SE (m a.s.l.)	Time to reach cone (s)
	V1	28	119	2200/4600	1885	40
	V2	37	100	2150/4400	1875	40
	V3	43	99	2140/4200	1850	45
	V4	41	89	2125/4100	1825	50
GJ	Multimat	40	120	2145/4300	1850	30
	V1	28	122	1950/4800	1850	45
	V2	36	106	1910/4450	1830	50
	V3	40	82	1900/4200	1825	55
	V4	39	99	1875/4100	1775	60
PJ	Multimat	41	113	1900/4200	1825	30

290

5. Discussion

5.1 Evolution of the Frébouge Cone

The different processes building up the Frébouge polygenetic cone and their timing provide important information and understanding on how the cone evolved. Our detailed mapping and chronology confirm the polygenetic origin of the Frébouge

295 cone by revealing its multi-origin composition, i.e. mainly made of sediments from rock avalanches, debris flows, glacial and fluvial processes. Its composition in combination with the cosmogenic [10]Be chronology suggests that the prevailing climate and surface processes changed with time. During the Last Glacial Maximum (LGM; 30 - 19 ka Ivy-Ochs, 2015), the Val Ferret and Val Veny were completely covered by ice, and the glacier reached Ivrea (Gianotti et al., 2008; Serra et al., 2022). During the cold period of the Younger Dryas (YD; 12.8 – 11.7 ka; Heiri et al., 2004), the ice surface in the Ferret Valley was up to an

300 elevation of 1950 m a.s.l. at Frébouge (Porter and Orombelli, 1982). The Frébouge cone is mainly composed of deposits from slope failures such as rock avalanches or debris flows, which are enhanced in the context of deglaciation (e.g., Cossart et al., 2008). Therefore, it is likely that the Frébouge cone started to build up during the paraglacial period (Ballantyne, 2002), when glaciers retreated to higher elevations and freed the valley. Although we cannot accurately underpin the beginning of the accumulation, considering the oldest debris flow nose on the southern side of the flank that we dated to 1900 ± 200 years, we

305 conclude that it should have started well prior as this debris flow at the surface of a cone is several tens of m thick. In addition, we identified pulses of debris flows occurring between 1200 ± 200 years and 800 ± 80 years ago.

17

1300 ± 100 years ago a rock avalanche with a volume possibly up to 12 Mm³ occurred, overriding an already existing cone, which was most likely composed of polygenetic deposits. We compared the timing of the Frébouge rock avalanche to glacier advances and rock avalanches reconstructed at Brenva and Triolet (Holzhauser et al., 2005; Nussbaumer et al., 2007; Arnaud

310   et al. 2012; Deline et al. 2015; Le Roy et al. 2015) (Figure 8). The Frébouge rock avalanche would have occurred when the glaciers started to retreat, after the glacier advance peak recorded around 1.4 ka at Mer de Glace (Le Roy et al., 2015) or Aletsch (Holzhauser et al., 2005) (Figure 8), during the Göschenen Cold Phase II (ca. 1.8–1.1 ka). Titanium anomalies measured in Lake Le Bourget (Savoie, France), indicating the terrigenous silicate input are high between 1450-1300 cal. BP, suggest a larger contribution of the catchments located at high elevations, which is associated with climatic changes such as

315   major glacier advances (Arnaud et al., 2012; Figure 8). Possible reasons for this timing after a glaciation are rock strength degradation due to pore pressure fluctuations or dynamic unloading during glacier melting (cf. Prager et al., 2008). Also, permafrost degradation starting at the beginning of the Holocene or associated groundwater regime changes should have led to an increase in rock avalanche activity (Dramis et al., 1995; Gruber and Haeberli, 2007; Parger et al., 2008; Ravanel et al., 2010). The Mer de Glace record shows stronger glacier fluctuations during the last 500 years and no clear correlation is

320   recognizable between the rock avalanches and the glacier extent (Figure 8). However, the Frébouge rock avalanche fits the major landslide period identified in the Italian Alps, which started 1500 years ago (Galadini et al., 2001; Sauro and Zampieri, 2001; Ivy-Ochs et al., 2017; Rossato et al., 2020; Viganò et al., 2021). For this rock avalanche period, neotectonic activity is assumed as the trigger (Galadini et al., 2001; Sauro and Zampieri, 2001). Furthermore, the Frébouge rock avalanche likely dammed the Doire River and led to the formation of the alluvial plain (Figure 3). Further evidence for the blocked Doire River

325   is given by the slightly higher ground surface in the northwest than at the alluvial plain because the ground surface on both sides of the river should theoretically be at the same elevation. In addition, a large boulder is embedded in sediments in the river bed.
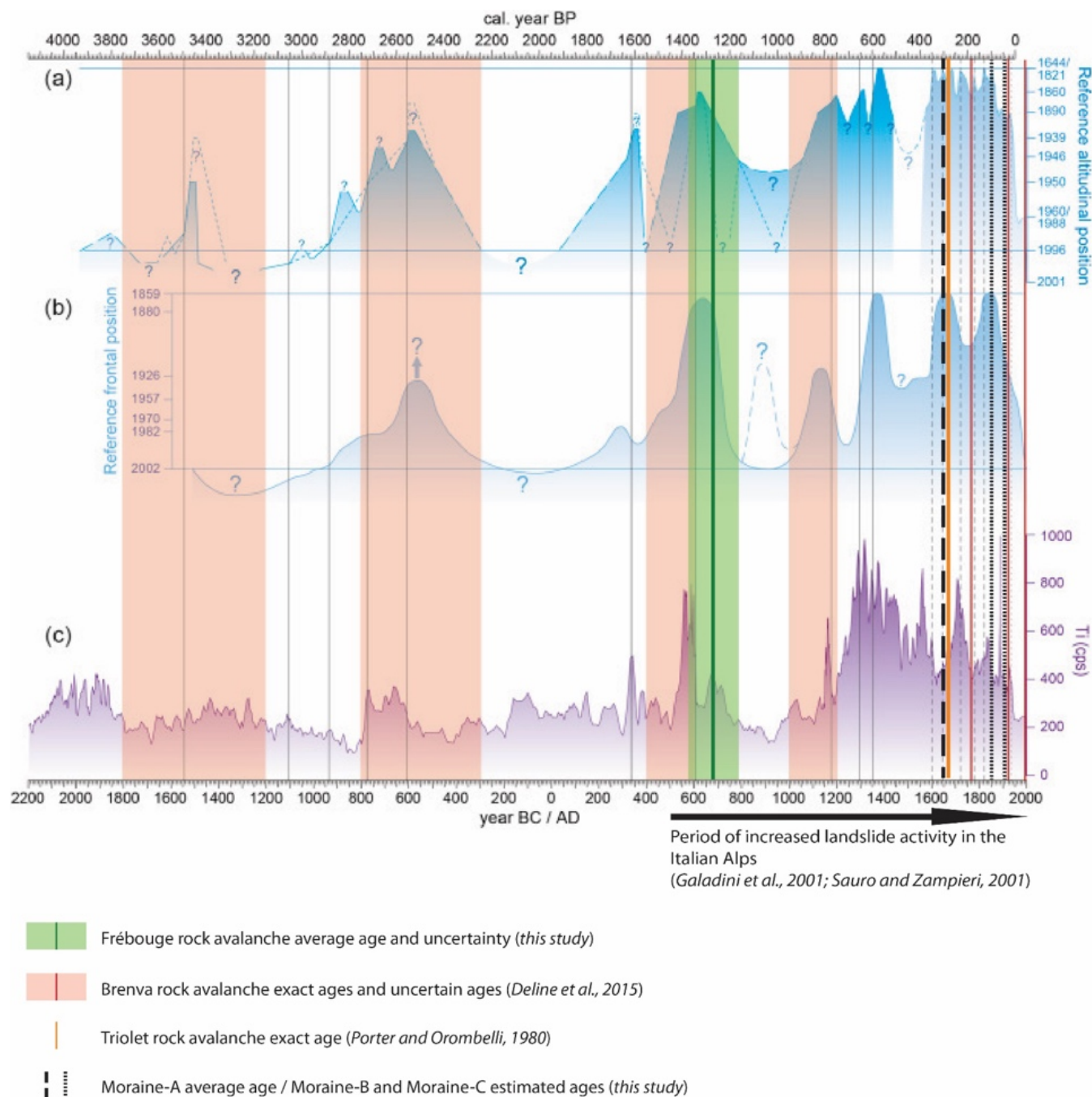
Figure 8: Comparison of the moraine chronology at Frébouge and the timing of the Frébouge rock avalanche to other rock avalanches in the Ferret and Veny valleys, glacier extends and lacustrine records (modified after Deline et al., 2015; Le Roy et al., 2015). a) Dendro-based chronology of advances of Mer de Glace (Mont Blanc massif) (Nussbaumer et al., 2007; Le Roy et al., 2015); b) Dendro-based chronology of advances of Great Aletsch Glacier (central Switzerland) (Holzhauser et al., 2005); c) Terrigenous input (titanium) in Lake Le Bourget (Savoie, France) as an indicator for glacial activity (Arnaud et al., 2012).

19

The Frébouge Glacier readvanced multiple times over the Frébouge cone and deposited till and moraines (Deline, 2009). The

335 largest readvance of the Frébouge Glacier occurred 320 ± 20 years ago, when Moraine-A was deposited (Figures 2, 6 and 8). A similar timing of glacier advances was also reported in Austria (Braumann et al., 2020, 2021), Central Alps (Kronig et al., 2018; Steinemann et al., 2021; Schimmelpfennig et al., 2022), and on the French side of the Mont Blanc Massif (Protin et al., 2021). The chronology of Great Aletsch Glacier advances shows that the glacier reached a maximum around 1660 AD (Holzhauser et al. 2005; Figure 8), while the Frébouge Glacier had its maximum at 1700 ± 20 AD. Moraine-B could correspond

340 to the glacier advance at ca. 1820 or 1850 AD (e.g. Holzhauser et al. 2005; Ivy-Ochs et al. 2009; Schimmelpfennig et al. 2012; Braumann et al., 2020). While the Great Aletsch Glacier had a similar size during its advance in middle 19th century as during the 1660 AD advance (Figure 8), the advance 320 ± 20 years ago at Frébouge was larger than the other LIA advances. Based on photographs, the uppermost moraine on the cone (Moraine-C) corresponds to a glacier advance in the early 20th century (Sacco, 1918; Gabinio, 1923). In contrast to the older debris flow deposits on the sides of the cone, the debris flow deposits in

345 the center of the cone cut the moraines and are therefore younger (Figures 3 and 4). Some of the debris flows on the sides of the cone possibly occurred after the LIA glacier advances, fed by water coming from the bedrock on the sides of the cone. Indicators for this scenario are the orientation of the debris flow levees and channels where some tend towards the bedrock lip. Today, debris flows occur in the central part of the cone. First, they follow the channels already cut into the moraines. Beyond the moraines, they are capable to deposit sediments without any obstacles. Evidence of snow avalanches is also found beyond

350 the moraine ridges. In the central part of the cone, shreds of evidence for repeated snow-avalanche activity are broken and moved boulders, as frequent snow avalanches in that zone do not allow trees to grow. One boulder was identified as an outlier (FREB-2: 500 ± 70 years) that is deposited among three older boulders (FREB-1, 3 and 4; Figure 3) because we think that it could have been moved by a snow avalanche 800 years after its deposition by the rock avalanche. Finally, the two other younger boulders, FREB-13 (300 ± 40 years) and FREB-14 (0.9 ± 0.2 ka), were identified as outliers. We argue that they could

355 attest to more recent and smaller rock avalanches because their displacement by a snow avalanche or a rockfall is very unlikely due to their size (e.g., FREB-14 is 14-m-long).

5.2 The Frébouge Rock Avalanche

Our detailed analysis has revealed that the Frébouge rock avalanche played an important role in the formation of the cone. The volume reconstruction revealed that this event initiated as a 9.5 Mm^3 failure, which then bulked to 12 Mm^3 and contributed a

360 large volume of sediment to the cone. However, there are some uncertainties associated with this volume reconstruction. When reconstructing the deposit, a hill in the topography, composed of argillaceous schist and siliceous limestone clasts (indicated by a gray colored dashed line in Figure 3), was included in the deposit volume. This hill could have been deposited during an earlier earth flow coming down the channel from the southeastern slope, and represents a volume of approximately 0.13 Mm^3 (Deline, 2009). To further explore the uncertainties in our reconstruction, we compared the reconstructed release volume of

365 9.5 Mm^3 to empirical correlations provided between source volume and deposit area (Griswold and Iverson 2008), as well as source volume and H/L glacier (Aaron and McDougall, 2019). Our reconstruction fits well with the Griswold and Iverson

(2008) data, however the H/L for the Frébouge rock avalanche suggests low mobility, despite the presence of both saturated substrate and glacial ice. This latter point is discussed below.

370   Our simulation results revealed that this large volume of sediment was delivered to the cone in a matter of minutes. These best fit Dan3D simulations well reproduce the simulation constraints, however there are some discrepancies with the field observations. The first is that the observed runup height of 150 m (1875 m a.s.l) above the valley floor was underestimated by about 25 m by the simulation. In the field, granitic boulders are present on the slope until 1875 m a.s.l., and a runup height of 150 m fits well with other documented runups produced by rock avalanches with highly elevated release areas comparable to the Grandes or Petites Jorasses (e.g., Evans et al. 1994). It is therefore likely that the simulation underestimates the runup,

375   which can be one limitation of using a depth-averaged numerical model and frictional/ Voellmy rheology (e.g. Aaron et al., 2020).

The modelled extent of the rock avalanche in the south-western part came to standstill further down valley than expected. This part of the Frébouge cone was strongly modified by glacier and debris flows since the rock avalanche occurred. A further indication for the extent is the location of the samples FREB-1 to FREB-7, which are covered by the simulated deposit extent.

380   Finally, the simulation does not reach the mapped boundary in the north and moved instead more down valley. This over 100 m smaller runout of the simulation is unlikely, as the rock avalanche deposit is clearly delineated by a 2m high rim at the edge of the cone from the surrounding deposits.

The debris flow sample FREB-15 has an age of 1900 ± 200 years and is therefore older than the rock avalanche. According to the simulation and the reconstructed topography, the rock avalanche deposit should be several meters thick at this location and

385   cover an older debris flow nose. Inheritance of this sample is unlikely, as the age is in a similar range as sample FREB-16, which has an exposure age of 1200 ± 200 years. Still the nose is striking out of the surrounding in field, which suggests, that the rock avalanche deposit is thinner on the side of the cone than shown by the simulation.

As mentioned above, the simulation covers a smaller area than the topographic reconstruction to get the same volume, primarily due to underestimation of the northeast deposits' extent. This smaller area was compensated with a larger thickness of the

390   deposit. Both have a maximal thickness of 40 m; however, the simulation has a larger area with thicknesses over 30 m compared to the topographic reconstruction. The maximal thickness of over 40 m is much larger than in the rock avalanches that travelled onto glacier in the Mont Blanc massif, where the thicknesses are typically between 1 to 5 m (Deline, 2009), and in other glaciated mountain ranges (Deline et al., 2021). In the southwestern part the thickness of the simulated rock avalanche has a smooth decrease in volume despite the presence of the aforementioned hill (Figures 3 and 7).

395   During the modelling a constant turbulence coefficient of 500 was used, and the best fit friction coefficient was found to be 0.2. Compared to best fitting Voellmy parameters in other rock avalanches on saturated sediment, the friction coefficient is slightly higher but within the range found for other events (Aaron and McDougall, 2019; Figure 9). This contrasts with the H7L correlation presented earlier, which suggests low mobility for this event. H/L can be confounded by geometric factors (e.g. Davies and McSaveney, 1999), and we consider the runout modelling results more reliable when placing the mobility of

400   the Frébouge rock avalanche in the context of other case histories.

Based on all this, we consider the reconstructed volume of 12 Mm^3 representing the upper bound. This supports the assumption that a release volume of 9.5 Mm^3 and deposition of volume 12 Mm^3 are in the upper range of realistic volumes of the Frébouge rock avalanche.
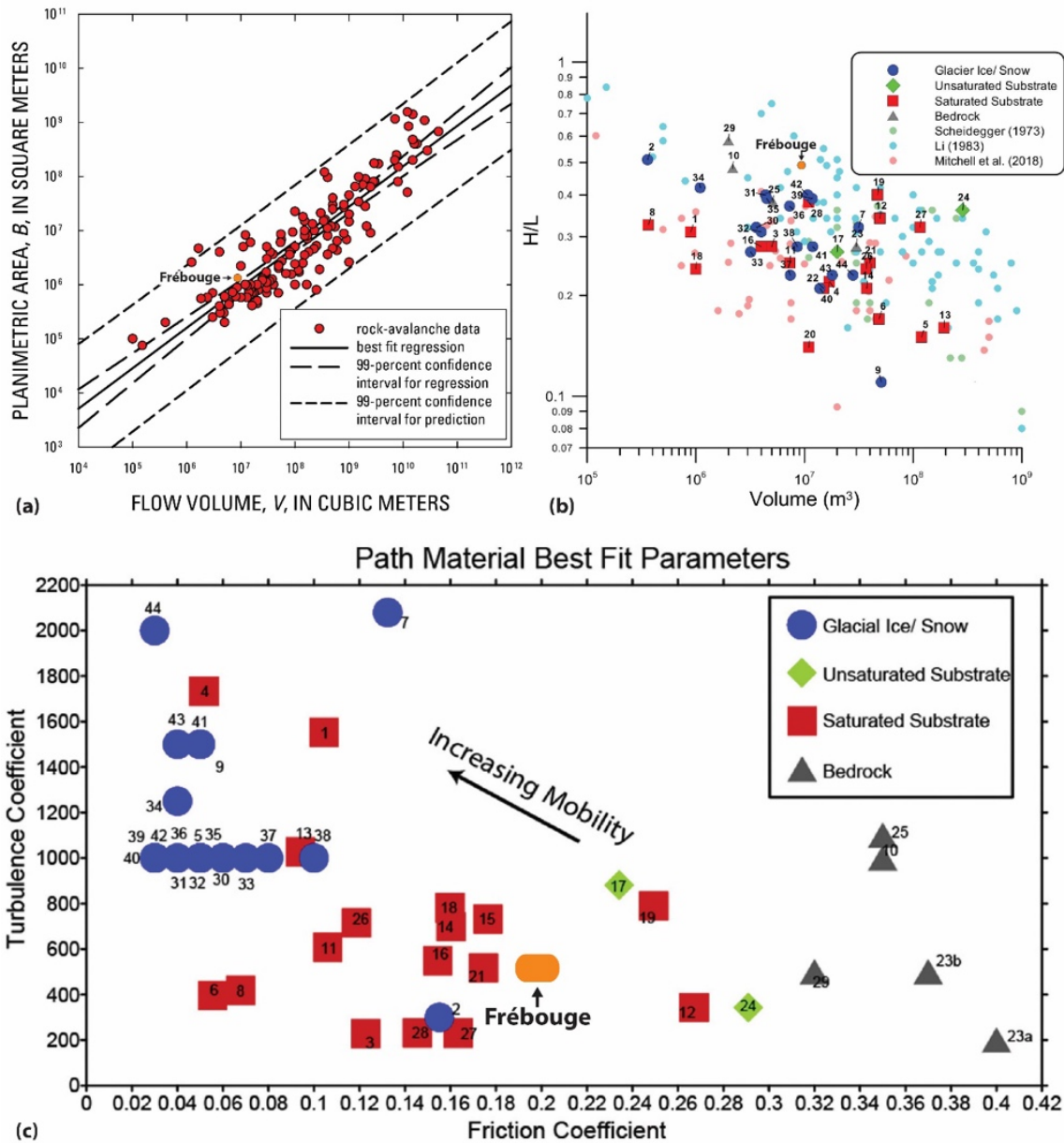
Figure 9: A) Rock avalanche data with the best-fitting regression line and the confidence interval compared to the Frébouge rock avalanche (modified after Griswold and Iverson, 2008). B) Volume vs. H/L plot of the Frébouge rock avalanche compared to a database of rock avalanches (modified after Aaron and McDougall, 2019). C) Collection of best-fitting Voellmy parameters for different path materials in comparison with the parameters used at the Frébouge rock avalanche (modified after Aaron and McDougall, 2019).

6. Conclusions

In this study, we investigated the evolution of the Frébouge polygenetic cone in the Ferret Valley based on geomorphological mapping, [10]Be surface exposure ages, and simulations of the rock avalanche. The geomorphological mapping revealed that the different deposits show complex interactions. Snow avalanche activity is indicated by cracked and cut trees and broken and displaced boulders. Moraines, till and debris flow deposits partially cover deposit of a large rock avalanche. The moraines indicate several Frébouge Glacier advances onto the cone, with a LIA maximal extent 320 ± 20 years ago. The oldest landforms on the Frébouge cone are the debris flow deposits on the southwestern side dated to 1900 ± 200 years. A rock avalanche with a maximum released volume of $9.5 \, \mathrm{Mm}^3$ occurred 1300 ± 100 years ago. Its source area in the Frébouge Glacier cirque remains unclear, as the simulations showed no difference in runout comparing different release areas.

The Frébouge rock avalanche may have occurred at the onset of glacier retreat during the Göschenen Cold Phase II, therefore possibly in connection with climate. Resulting glacier or pore pressure fluctuations were suggested as possible triggers for rock avalanches (Prager et al. 2008). Furthermore, the Frébouge rock avalanche is contemporaneous with increased landslide activity identified in northern Italy, which was assigned to regional neotectonic activity. Beside climate related factors, tectonics as a trigger is therefore also conceivable. With ongoing global warming, the size of proglacial and polygenetic landscapes will grow. Therefore, studying the evolution of further polygenetic landscapes to understand the interactions and the timing of the different processes and to predict future hazards caused by debris flows or rock avalanches in similar settings is of increasing importance as slope failures can cause severe damages to settlements and infrastructure located close by.

Author contribution

The research concept was designed by NA, SIO and PD. PH, PD, SIO, and NA conducted fieldwork and collected samples for surface exposure dating. The samples were processed in the laboratory by CD and PH. JA and PH performed the runout modelling. MC measured the [10]Be at the AMS facility in Zurich. CD, PH, PD, SIO, JA, and NA analysed and interpreted the data. CD drafted the manuscript and figures with contributions from all authors. The manuscript was read and approved by all authors.

Data availability

All data generated or analysed during this study are included in this article.

Competing interests

The authors declare that they have no conflict of interest.

References

Aaron, J. and Hungr, O.. Dynamic simulation of the motion of partially-coherent landslides, Eng. Geol., 205, 1-11, doi:10.1016/j.enggeo.2016.02.006, 2016.

Aaron, J. and McDougall, S.: Rock avalanche mobility: The role of path material, Eng. Geol., 257, 105126,
450   doi:10.1016/j.enggeo.2019.05.003, 2019.

Aaron, J., McDougall, S. and Nolde, N.:Two methodologies to calibrate landslide runout models, Landslides, 16(5), 907-920, doi:10.1007/s10346-018-1116-8, 2019.

Aaron, J., McDougall, S., and Jordan, P.: Dynamic analysis of the 2012 Johnsons Landing landslide at Kootenay Lake, British Columbia: The importance of undrained flow potential, Can. Geotech. J., 57(8), 1172-1182, https://doi.org/10.1139/cgj-2018-
455   0623, 2020.

Aaron, J., McDougall, S., Kowalski, J., Mitchell, A., and Nolde, N.: Probabilistic prediction of rock avalanche runout using a numerical model, Landslides 19, 2853–2869, https://doi.org/10.1007/s10346-022-01939-y, 2022.

Akçar, N., Ivy-Ochs, S., Kubik, P. W. and Schlüchter, C.: Post-depositional impacts on 'Findlinge' (erratic boulders) and their implications for surface-exposure dating. Swiss J Geosci, 104(3), 445-453, doi:10.1007/s00015-011-0088-7, 2011.

460   Akçar, N., Deline, P., Ivy-Ochs, S., Alfimov, V., Hajdas, I., Kubik, P. W., Christl, M. and Schlüchter, C.: The AD 1717 rock avalanche deposits in the upper Ferret Valley (Italy): a dating approach with cosmogenic 10 Be, J. Quat. Sci., 27(4), 383-392, doi:10.1002/jqs.1558, 2012.

Akçar, N., Ivy-Ochs, S., Deline, P., Alfimov, V., Kubik, P.W., Christl, M., and Schlüchter C.: Minor inheritance inhibits the calibration of the ^{10}Be production rate from the AD 1717 Val Ferret rock avalanche, European Alps, J. Quat. Sci., 29(4) 318-
465   328, doi:10.1002/jqs.2706, 2014

Akçar, N., Ivy-Ochs, S., Alfimov, V., Schlunegger, F., Claude, A., Reber, R., Christl, M., Vockenhuber, C., Dehnert, A., Rahn, M., and Schlüchter, C.: Isochron-burial dating of glaciofluvial deposits: First results from the Swiss Alps, Earth Surf. Process. Landf., 42(14), 2414–2425, doi.org/10.1002/esp.4201, 2017.

André, M. F.: Rates of Postglacial rock weathering on glacially scoured outcrops (Abisko–Riksgränsen area, 68°N), Geogr.

470   Ann. Ser. A-phys. Geogr., 84(3-4), 139-150, doi:https://doi.org/10.1111/j.0435-3676.2002.00168.x, 2002.

Arnaud, F., Révillon, S., Debret, M., Revel, M., Chapron, E., Jacob, J., Giguet-Covex, C., Poulenard, J. and Magny, M.: Lake Bourget regional erosion patterns reconstruction reveals Holocene NW European Alps soil evolution and paleohydrology. Quat. Sci. Rev, 51, 81-92, doi:https://doi.org/10.1016/j.quascirev.2012.07.025, 2012.

Balco, G., Stone, J. O., Lifton, N. A. and Dunai, T. J.: A complete and easily accessible means of calculating surface exposure

475   ages or erosion rates from [10]Be and [26]Al measurements. Quat. Geochronol., 3(3), 174-195, doi:https://doi.org/10.1016/j.quageo.2007.12.001, 2008.

Ballantyne, C. K.: A general model of paraglacial landscape response, The Holocene, 12(3), 371-376, doi:10.1191/0959683602hl553fa, 2002.

Bini A, Buonchristiani JF, Couterand S, Ellwanger D, Felber M, Florineth D, Graf HR, Keller O, Kelly M, Schlüchter C,

480   Schöneich P.:In Die Schweiz während des letzteiszeitlichen Maximums (LGM), Burkhalter R (Ed). Federal Office of Topography, swisstopo: CH-3084 Wabern, Bern., 2009.

Bishop, M., and Dobreva, I.: Geomorphometry and Mountain Geodynamics: Issues of Scale and Complexity, in: Integrating Scale in Remote Sensing and GIS, edited by: Quattrochi, D. A., Wentz, E., Siu-Ngan L. N., and Emerson, C. W., CRC Press, 189-228, https://doi.org/10.1201/9781315373720.

485   Braumann, S. M., Schaefer, J. M., Neuhuber, S. M., Reitner, J. M., Lüthgens, C., and Fiebig, M.: Holocene glacier change in the Silvretta Massif (Austrian Alps) constrained by a new [10]Be chronology, historical records and modern observations, Quaternary Sci. Rev., 245, 106493, https://doi.org/10.1016/j.quascirev.2020.106493, 2020.

Braumann, S. M., Schaefer, J. M., Neuhuber, S. M., Lüthgens, C., Hidy, A. J., and Fiebig, M.: Early Holocene cold snaps and their expression in the moraine record of the eastern European Alps, Clim. Past, 17, 2451–2479, https://doi.org/10.5194/cp-

490   17-2451-2021, 2021.

Carrivick, J. L., Geilhausen, M., Warburton, J., Dickson, N. E., Carver, S. J., Evans, A. J. and Brown, L. E.: Contemporary geomorphological activity throughout the proglacial area of an alpine catchment, Geomorphology, 188, 83-95, doi:https://doi.org/10.1016/j.geomorph.2012.03.029, 2013.

Carrivick, J. L., Heckmann, T., Fischer, M. and Davies, B.: An Inventory of Proglacial Systems in Austria, Switzerland and

495   Across Patagonia, in: Geomorphology of Proglacial Systems, edited by: Heckmann T. and Morche D.. Springer Cham, 43-57, https://doi.org/10.1007/978-3-319-94184-4_3, 2019.

Chmeleff, J., von Blanckenburg, F., Kossert, K. and Jakob, D.: Determination of the [10]Be half-life by multicollector ICP-MS and liquid scintillation counting, Nucl Instrum Methods Phys Res B Nucl. Instrum. Meth. B, 268(2), 192-199, doi:https://doi.org/10.1016/j.nimb.2009.09.012, 2010.

500   Christl, M., Vockenhuber, C., Kubik, P. W., Wacker, L., Lachner, J., Alfimov, V. and Synal, H. A.: The ETH Zurich AMS facilities: Performance parameters and reference materials. Nucl Instrum Methods Phys Res B Nucl. Instrum. Meth. B, 294, 29-38, doi:https://doi.org/10.1016/j.nimb.2012.03.004, 2013.

Cossart, E., Braucher, R., Fort, M., Bourle´s, D.L., Carcaillet, J.: Slope instability in relation to glacial debuttressing in alpine areas (Upper Durance catchment, southeastern France): evidence from field data and [10]Be cosmic ray exposure ages,

505   Geomorphology, 95, 3-26, https://doi.org/10.1016/j.geomorph.2006.12.022, 2008.

Costa, A., Molnar, P., Stutenbecker, L., Bakker, M., Silva, T.A., Schlunegger, F., Lane, S.N., Loizeau, J.-L., and Girardclos, S.: Temperature signal in suspended sediment export from an Alpine Catchment, Hydrol. Earth Syst. Sci., 22, 509–528, doi.org/10.5194/hess-22-509-2018, 2018.

Davies, T. R., and McSaveney, M. J.: Runout of dry granular avalanches, Can. Geotech. J., 36(2), 313-320,

510   https://doi.org/10.1139/t98-108, 1999.

Deline, P.: Interactions between rock avalanches and glaciers in the Mont Blanc massif during the late Holocene. Quat. Sci. Rev., 28(11-12), 1070-1083, doi:10.1016/j.quascirev.2008.09.025, 2009.

Deline, P. and Kirkbride, M. P.: Rock avalanches on a glacier and morainic complex in Haut Val Ferret (Mont Blanc Massif, Italy), Geomorphology, 103(1), 80-92, doi:https://doi.org/10.1016/j.geomorph.2007.10.020, 2009.

515   Deline, P., Chiarle, M., Mortara, G.: The front ice avalanche of Frébouge Glacier (Mont Blanc Massif, Valley of Aosta) on 18 September 2002. Geogr. Fis. Dinam. Quat., 25(2), 101–104, 2002.

Deline, P., Chiarle, M. and Mortara, G.: The July 2003 Frebouge debris flows (Mont Blanc Massif, valley of Aosta, Italy): Water pocket outburst flood and ice avalanche damming, Geogr. Fis. Dinam. Quat., 27, 107-111, 2004.

Deline, P., Gardent, M., Magnin, F. and Ravanel, L.: The morphodynamics of the Mont Blanc Massif in a changing cryosphere:

520   a comprehensive review.), Geogr. Ann. Ser. A-phys. Geogr., 94(2), 265-283, doi:10.1111/j.1468-0459.2012.00467.x, 2012.

Deline, P., Akçar, N., Ivy-Ochs, S. and Kubik, P. W. (2015). Repeated Holocene rock avalanches onto the Brenva Glacier, Mont Blanc massif, Italy: A chronology. Quat. Sci. Rev., 126, 186-200, doi:https://doi.org/10.1016/j.quascirev.2015.09.004, 2015.

Deline, P., Hewitt, K., Reznichenko, N. and Shugar, D.: Chapter 9 - Rock Avalanches onto Glaciers, in: Landslide Hazards,

525   Risks and Disasters, 2nd edition, edited by: Davies, T.R.H., Rosser, N., Elsevier, Amsterdam, 269-333, 9780128184646, 2021.

Dramis, F., Govi, M., Guglielmin, M. and Mortara, G.: Mountain permafrost and slope instability in the Italian Alps: The Val Pola Landslide, Permafrost and Periglacial Process., 6(1), 73-81, doi:https://doi.org/10.1002/ppp.3430060108, 1995.

Dunne, J., Elmore, D. and Muzikar, P.: Scaling factors for the rates of production of cosmogenic nuclides for geometric shielding and attenuation at depth on sloped surfaces, Geomorphology, 27(1), 3-11, doi:https://doi.org/10.1016/S0169-

530   555X(98)00086-5, 1999.

Dortch, J.M., Tomkins, M.D., Saha, S., Murari, M.K., Schoenbohm, L.M., Curl, D.,: A tool for the ages: The Probabilistic Cosmogenic Age Analysis Tool (P-CAAT), . Quat. Geochronol., 71, 101323, 2022.

Evans, S. G., Hungr, O. and Enegren, E. G.: The Avalanche Lake rock avalanche, Mackenzie Mountains, Northwest Territories, Canada: description, dating, and dynamics. Can. Geotech. J., 31(5), 749-768, doi:10.1139/t94-086, 1994.

535   Gabinio, M.: Mario Gabinio Collection. in: Torino Civic Gallery of Modern and Contemporary Art (GAM), 1923.

Galadini, F., Galli, P., Cittadini, A. and Giaccio, B.: Late Quaternary fault movements in the Mt. Baldo-Lessini Mts sector of the Southalpine area (northern Italy), Neth. J. Geosci., 80(3-4), 187-208, doi:10.1017/S0016774600023830, 2001.

Giambastiani, M.: Valutazione geomorfologica del rischio di frana, di valanga e di piena di rotta glaciale in un'area alpina (Courmayeur, Valle d'Aosta, Geologia Tecnica, 2, 5-16, 1983.

540 Gianotti, F., Forno, M.G., Ivy-Ochs, S. and Kubik, P.W.: New chronological and stratigraphical data on the Ivrea amphitheatre (Piedmont, NW Italy), Quat. Int., 190(1), 123-135, https://doi.org/10.1016/j.quaint.2008.03.001, 2008.

Grämiger, L. M., Moore, J. R., Vockenhuber, C., Aaron, J., Hajdas, I. and Ivy-Ochs, S.: Two early Holocene rock avalanches in the Bernese Alps (Rinderhorn, Switzerland), Geomorphology, 268, 207-221, doi:https://doi.org/10.1016/j.geomorph.2016.06.008, 2016.

545 Griffith, J. S., Smith, M. J. and Paron, P.: Introduction to Applied Geomorphological Mapping. In: Geomorphological Mapping – Methods and Applications, edited by: Mike J. Smith, M.J., Paron, P., James S., and Griffiths, J.S., Elsevier, Amsterdam, 3-11, 9780444534460 ,2011.

Griswold, J. P. and Iverson, R. M.: Mobility statistics and automated hazard mapping for debris flows and rock avalanches, Scientific Investigations Report 2007-5276, retrieved from Reston, VA: http://pubs.er.usgs.gov/publication/sir20075276,
550 2008.

Gruber, S. and Haeberli, W.: Permafrost in steep bedrock slopes and its temperature-related destabilization following climate change, J. Geophys. Res. F: Earth Surf., 112, F02S18, doi:https://doi.org/10.1029/2006JF000547, 2007.

Hallet, B., Hunter, L. and Bogen, J.: Rates of erosion and sediment evacuation by glaciers: A review of field data and their implications, Glob. Planet. Chang., 12(1), 213-235, doi:https://doi.org/10.1016/0921-8181(95)00021-6, 1996.

555 Heckmann, T. and Morche, D. (Eds): Geomorphology of Proglacial Systems: Landform and Sediment Dynamics, in: Recently Deglaciated Alpine Landscapes Springer, Cham, Switzerland, 361 pp., ISBN 978-3-319-94182-0, 2019.

Heiri, O., Koinig, K.A., Spötl, C., Barrett, S., Brauer, A., Drescher-Schneider, R., Gaar, D., Ivy-Ochs, S., Kerschner, H., Luetscher, M., Moran, A., Nicolussi, K., Preusser, F., Schmidt, R., Schoeneich, P., Schw€orer, C., Sprafke, T., Terhorst, B. and Tinner, W.: Palaeoclimate records 60-8 ka in the Austrian and Swiss Alps and their forelands. Quat. Sci.Rev. 106, 186-
560 205, https://doi.org/10.1016/j.quascirev.2014.05.021, 2014.

Holzhauser, H., Magny, M. and Zumbuühl, H. J.: Glacier and lake-level variations in west-central Europe over the last 3500 years. The Holocene, 15(6), 789-801, doi:10.1191/0959683605hl853ra, 2005.

Hungr, O. and Evans, S. G.: Entrainment of debris in rock avalanches: An analysis of a long run-out mechanism. Geol. Soc. Am. Bull., 116(9-10), 1240-1252, doi:10.1130/B25362.1, 2004

565 Ivy-Ochs, S. and Schaller, M.: Chapter 6 Examining Processes and Rates of Landscape Change with Cosmogenic Radionuclides, in Radioactivity in the Environment, edited by: Froehlich, K., Elsevier, 231-294, https://doi.org/10.1016/S1569-4860(09)01606-4, 2009.

Ivy-Ochs, S., Kerschner, H., Maisch, M., Christl, M., Kubik, P. W. and Schlüchter, C.: Latest Pleistocene and Holocene glacier variations in the European Alps, Quat. Sci. Rev., 28(21), 2137-2149, doi:https://doi.org/10.1016/j.quascirev.2009.03.009, 2009.

Ivy-Ochs S.: Glacier variations in the European Alps at the end of the last glaciation, Cuad. de Investig. Geogr., 41(2), 295-315, doi:10.18172/cig.2750, 2015.

Ivy-Ochs, S., Martin, S., Campedel, P., Hippe, K., Alfimov, V., Vockenhuber, C., Andreotti, E., Carugati, G., Pasqual, D., Rigo, M. and Viganò, A.: Geomorphology and age of the Marocche di Dro rock avalanches (Trentino, Italy). Quat. Sci. Rev., 169, 188-205, doi:https://doi.org/10.1016/j.quascirev.2017.05.014, 2017.

Kamp, U. and Owen, L. A.: 5.16 Polygenetic Landscapes, in: Treatise on Geomorphology, edited by: Shroder, J. F., Academic Press, San Diego, 370-393, 2013.

Kohl, C. P. and Nishiizumi, K.: Chemical isolation of quartz for measurement of in-situ -produced cosmogenic nuclides, Geochim. Cosmochim. Acta, 56(9), 3583-3587, doi:https://doi.org/10.1016/0016-7037(92)90401-4, 1992.

Korschinek, G., Bergmaier, A., Faestermann, T., Gerstmann, U. C., Knie, K., Rugel, G., Wallner, A., Dillmann, I, Dollinger, G., von Gostomski, C. L., Kossert, K., Maiti, M., Poutivtsev, M. and Remmert, A.: A new value for the half-life of ^{10}Be by Heavy-Ion Elastic Recoil Detection and liquid scintillation counting, Nucl Instrum Methods Phys Res B Nucl. Instrum. Meth. B, 268(2), 187-191, doi:https://doi.org/10.1016/j.nimb.2009.09.020, 2010.

Kronig, O., Ivy-Ochs, S., Hajdas, I., Christl, M., Wirsig, C., and Schlüchter, C.: Holocene evolution of the Triftje- and the Oberseegletscher (Swiss Alps) constrained with ^{10}Be exposure and radiocarbon dating. Swiss J Geosci 111, 117–131, https://doi.org/10.1007/s00015-017-0288-x, 2018.

Kubik, P. W. and Christl, M.: ^{10}Be and ^{26}Al measurements at the Zurich 6MV Tandem AMS facility, Nucl Instrum Methods Phys Res B Nucl. Instrum. Meth. B, 268(7), 880-883, https://doi.org/10.1016/j.nimb.2009.10.054, 2010.

Lal, D.: Cosmic ray labeling of erosion surfaces: in situ nuclide production rates and erosion models. Earth Planet. Sci. Lett., 104(2), 424-439, doi:https://doi.org/10.1016/0012-821X(91)90220-C, 1991.

Le Roy, M., Nicolussi, K., Deline, P., Astrade, L., Edouard, J.-L., Miramont, C. and Arnaud, F.: Calendar-dated glacier variations in the western European Alps during the Neoglacial: the Mer de Glace record, Mont Blanc massif, Quat. Sci. Rev., 108, 1-22, doi:10.1016/j.quascirev.2014.10.033, 2015.

Maizels, J.K., (1979). Proglacial Aggradation and Changes in Braided Channel Patterns during a Period of Glacier Advance : An Alpine Example, Geogr. Ann. Ser. A-phys. Geogr., 61(1), 87-101, 1979.

Marro, C. (1986). Les granitoïdes du Mont-Blanc en Suisse, PhD Thesis, University of Fribourg, 1986.

Maxeiner, S., Synal, H.-A., Christl, M., Suter, M., Müller, A. and Vockenhuber, C.: Proof-of-principle of a compact 300 kV multi-isotope AMS facility, Nucl Instrum Methods Phys Res B Nucl. Instrum. Meth. B, 439, 84-89, doi:https://doi.org/10.1016/j.nimb.2018.11.028, 2019.

McDougall, S. and Hungr, O.: A model for the analysis of rapid landslide motion across three-dimensional terrain, Can. Geotech. J., 41(6), 1084-1097, doi:10.1139/t04-052, 2004.

Nussbaumer, S. U., Zumbühl, H. J. and Steiner, D.: Fluctuations of the Mer de Glace (Mont Blanc area, France) AD 1500-2050: an interdisciplinary approach using new historical data and neural network simulations, Z. Gletsch.kd. Glazialgeol., 40 (2005/2006), 2007.

605 Penck, A., and Brückner, E.(Eds.): Die Alpen im Eiszeitalter, H.Tauchnitz, Leipzig, Germany, 1199pp, 1909.

Porter, S. C., and Orombelli, G.: Catastrophic Rockfall of September 12, 1717 on the Italian Flank of the Mont Blanc Massif, Z. Geomorphol., 24, 200–218, https://doi.org/10.1127/zfg/24/1984/200, 1980.

Porter, S. C., and Orombelli, G.: Alpine Rockfall Hazards: Recognition and dating of rockfall deposits in the western Italian Alps lead to an understanding of the potential hazards of giant rockfalls in mountainous regions, Am. Sci., 69(1), 67-75, 1981.

610 Porter, S. C., and Orombelli, G.: Late-glacial ice advances in the western Italian Alps, Boreas, 11(2), 125-140, doi:https://doi.org/10.1111/j.1502-3885.1982.tb00530.x, 1982.

Prager, C., Zangerl, C., Patzelt, G., and Brandner, R.: Age distribution of fossil landslides in the Tyrol (Austria) and its surrounding areas, Nat. Hazards Earth Syst. Sci., 8(2), 377-407, doi:10.5194/nhess-8-377-2008, 2008.

Protin,M., Schimmelpfennig, I., Mugnier, J.-L., Buoncristiani, J.-F., LeRoy,M., Pohl,B., Moreau, L., and ASTERTeam:
615 Millennial-scale deglaciation across the European Alps at the transition between the Younger Dryas and the Early Holocene – evidence from a new cosmogenic nuclide chronology, Boreas, 50, 671–685. https://doi.org/10.1111/bor.12519. ISSN 0300-9483, 2021.

Ravanel, L., Allignol, F., Deline, P., Gruber, S., and Ravello, M.: Rock falls in the Mont Blanc Massif in 2007 and 2008, Landslides, 7(4), 493-501, https://doi.org/10.1007/s10346-010-0206-z, 2010.

620 Rossato, S., Ivy-Ochs, S., Martin, S., Viganò, A., Vockenhuber, C., Rigo, M., Monegato, G., De Zorzi, M., Surian, N., Campedel, P. and Mozzi, P.: Timing, drivers and impacts of the historic Masiere di Vedana rock avalanche (Belluno Dolomites, NE Italy), Nat. Hazards Earth Syst. Sci., 20(8), 2157-2174, doi:10.5194/nhess-20-2157-2020, 2020.

Sacco, F.: I ghiacciai italiani del gruppo del Monte Bianco, Bolletino del Comitato Glaciologico Italiano, 3, 21-102, 1918.

Sauro, U. and Zampieri, D.: Evidence of recent surface faulting and surface rupture in the Fore-Alps of Veneto and Trentino
625 (NE Italy), Geomorphology, 40(3), 169-184, doi:https://doi.org/10.1016/S0169-555X(01)00041-1, 2001.

Schimmelpfennig, I., Schaefer, J. M., Lamp, J., Godard, V., Schwartz, R., Bard, E., Tuna, T., Akçar, N., Schlüchter, C., Zimmerman, S., and ASTER Team: Glacier response to Holocene warmth inferred from in situ [10]Be and ^{14}C bedrock analyses in Steingletscher's forefield (central Swiss Alps), Clim. Past, 18, 23–44, https://doi.org/10.5194/cp-18-23-2022, 2022.

Seijmonsbergen: 14.4 The Modern Geomorphological Map in: Treatise on Geomorphology, edited by: Shroder, J. F.,
630 Academic Press, San Diego, 35-52, 2013.

Serra, E., Valla, P.G., Gribenski, N., Carcaillet, J., Deline, P.: Post-LGM glacial and geomorphic evolution of the Dora Baltea valley (western Italian Alps), Quat. Sci. Rev., 282, 107446, 2022.

Slaymaker, O.: Criteria to distinguish between periglacial, proglacial and paraglacial environments, Quaest. Geogr., 30(1), 85-94, https://doi.org/10.2478/v10117-011-0008-y, 2011.

635 Sosio, R., Crosta, G. B., Chen, J. H. and Hungr, O.: Modelling rock avalanche propagation onto glaciers, Quat. Sci. Rev., 47, 23-40, doi:10.1016/j.quascirev.2012.05.010, 2012.

Steinemann, O., Ivy-Ochs, S., Hippe, K., Christl, M., Haghipour, N., and Synal, H. A.: Glacial erosion by the Trift glacier (Switzerland): Deciphering the development of riegels, rock basins and gorges, Geomorphology, 375, 107533, https://doi.org/10.1016/j.geomorph.2020.107533, 2021.

640 Stone, J. O.: Air pressure and cosmogenic isotope production, J. Geophys. Res. Solid Earth, 105(B10), 23753-23759, doi:10.1029/2000jb900181, 2000.

swisstopo: Geologische Karte der Schweiz 1:500 000, Bundesamt für Landestopographie swisstopo, Map, 2005

Viganò, A., Rossato, S., Martin, S., Ivy-Ochs, S., Zampieri, D., Rigo, M. and Monegato, G.: Large landslides in the Alpine valleys of the Giudicarie and Schio-Vicenza tectonic domains (NE Italy), J. Maps, 1-12, doi:10.1080/17445647.2021.1880979, 645 2021.

Wirsig, C., Zasadni, J., Christl, M., Akçar, N. and Ivy-Ochs, S.: Dating the onset of LGM ice surface lowering in the High Alps, Quat. Sci. Rev., 143, 37-50, doi:https://doi.org/10.1016/j.quascirev.2016.05.001, 2016.